Spin wave interactions in the pyrochlore Heisenberg antiferromagnet with Dzyaloshinskii-Moriya interactions

V. V. Jyothis,[1,*] Kallol Mondal,[1,2,†] Himanshu Mavani,[1,3,‡] and V. Ravi Chandra[1,§]

[1]*School of Physical Sciences, National Institute of Science Education and Research Bhubaneswar, Jatni, Odisha 752050, India and Homi Bhabha National Institute, Training School Complex, Anushaktinagar, Mumbai 400094, India*

[2]*AGH University of Krakow, Faculty of Physics and Applied Computer Science, Aleja Mickiewicza 30, 30-059 Krakow, Poland*

[3]*Department of Physics and Astronomy and Nebraska Center for Materials and Nanoscience, University of Nebraska, Lincoln, Nebraska 68588-0299, USA*

(Received 28 February 2025; revised 14 May 2026; accepted 1 July 2026; published 22 July 2026)

We study the effect of magnon interactions on the spin wave spectra of the all-in-all-out phase of the pyrochlore nearest neighbor antiferromagnet with a Dzyaloshinskii-Moriya interaction (D). The leading order corrections to spin wave energies indicate a significant renormalization for commonly encountered strengths of the Dzyaloshinskii-Moriya term. For low values of D we find a potential instability of the phase itself, indicated by the renormalization of magnon frequencies to negative values. We have also studied the renormalized spectra in the presence of magnetic fields along three high symmetry directions of the lattice, namely, the [111], [100], and [110] directions. Generically, we find that for a fixed value of the Dzyaloshinskii-Moriya interaction renormalized spectra for the lowest band decrease with an increasing strength of the field. We have also analyzed the limits of the two-magnon continuum and probed the possibility of magnon decay. For a range of D and the field strength we identify possible parameter regimes where the decay of the higher bands of the system are kinematically allowed.

DOI: 10.1103/bjjx-hhl6

I. INTRODUCTION

The study of the effects of interactions between magnons is nearly as old as the description of magnons as the lowest excitations in ordered magnets. After early descriptions of spin waves as elementary excitations of ordered ferromagnets [1] and antiferromagnets [2,3], detailed analyses of magnon interactions in both ferromagnets and antiferromagnets were presented [4–6]. Most of these early efforts were focused on the effect of spin wave interactions in spin models with collinear magnetic order, usually for lattices with cubic symmetry and purely Heisenberg interactions. For such cases, at least at low temperatures, it was concluded that the phases could be described fairly accurately using noninteracting magnons. For instance, the results for relevant physical quantities like magnetization, specific heat, susceptibility, etc., do not deviate from those of linear spin wave theory (LSWT) beyond a few percent if the leading corrections due to magnon interactions are taken into account [4–6].

Many of the ordered magnetic materials and the model Hamiltonians of interest currently do not possess the above mentioned characteristics that render spin wave interactions irrelevant. In the present day, there is a lot of interest in the kind of magnetic order which is not a standalone phase but rather competes with other ordered phases or spin liquid states. Furthermore, the occurence of collinear order (moments pointing along or opposite to a single direction) is more likely to be a feature of spin models with a bipartite lattice structure and short range interactions. Many of the contemporary magnetic Hamiltonians that have long range magnetic order have noncollinear ordering patterns, either because of multiple coupling constants or geometrical frustration or both. Finally, the analysis of many measurements requires considerations of excitations of spin models away from the lowest temperatures. Magnon interactions can in principle play a significant role in all such circumstances. The effect of spin wave interactions in such systems is far from benign and can lead to substantial spectral renormalization and additional effects like spontaneous decay of magnons [7,8].

Most of the above reasons to study spin wave interactions can arise simultaneously in spin models on the pyrochlore lattice. It is one of the most widely studied platforms to probe the effect of geometrical frustration on magnetic order. The $A_2B_2O_7$ class of materials provides an array of possible material realizations [9]. Furthermore, this lattice also proved to be the source of one of the first topological magnonic band structures investigated [10], where a nonvanishing thermal Hall conductivity was explained using a finite Berry curvature of the spin wave bands. In this context, it is important to note that while understanding of spin wave interactions is relevant and important in its own right, interest in the same has also witnessed a resurgence recently because of the interest in studying topological magnonic band structures [11–13]. Much of the analysis of topological magnons relies on the

*Contact author: jyothis.vv@niser.ac.in
†Contact author: kmondal@agh.edu.pl
‡Contact author: hmavani2@huskers.unl.edu
§Contact author: ravi@niser.ac.in

magnon band structure at the noninteracting level. However, the emergence of topologically nontrivial spin wave band structures often involves noncollinear magnetic order and/or geometrically frustrated lattices, circumstances in which deviations from linear spin wave theory are frequently found. As a result there have been several recent attempts to ascertain the effect of interactions on the predictions of topological magnonic theories, mostly for two-dimensional Hamiltonians [14–22].

The lattice structure of the pyrochlore allows for anisotropic interactions like the Dzyaloshinskii-Moriya interaction (DMI) and local spin anisotropies which make it a very suitable system for noncollinear low temperature phases and thence for the study of magnon interactions. Existing works on the effect of spin wave interactions in this lattice have focused on different aspects of the ferromagnetic phase [23,24]. In this work we initiate a study of the effect of spin wave interactions in a spin model on the pyrochlore lattice with antiferromagnetic Heisenberg exchange and Dzyaloshinskii-Moriya interactions. We study the all-in-all-out (AIAO) phase of this lattice and the effect of magnon interactions on spin wave spectra of this phase. Several aspects of the magnon spectra of this phase both in the bulk and the thin film limits have been studied recently [25,25–29]. The frequent occurrence of this phase in the pyrochlore lattice and the nature of the phase itself make it an important target for the investigation of spin wave interactions.

II. MODEL HAMILTONIAN AND FORMALISM

The model Hamiltonian we study has the form

$$H = J \sum_{\langle i\alpha, j\beta\rangle} \mathbf{S}_{i\alpha} \cdot \mathbf{S}_{j\beta} + \sum_{\langle i\alpha, j\beta\rangle} \mathbf{D}_{i\alpha,j\beta} \cdot (\mathbf{S}_{i\alpha} \times \mathbf{S}_{j\beta}) - \sum_{i\alpha} \mathbf{B} \cdot \mathbf{S}_{i\alpha}. \tag{1}$$

Here $\mathbf{S}_{i\alpha}$ are spins on the sites of the pyrochlore lattice and the first subscript denotes the Bravais lattice index and the Greek index denotes one of the four sublattices. J and $\mathbf{D}_{i\alpha,j\beta}$ are the coefficients of the Heisenberg exchange and Dzyaloshinskii-Moriya interactions [30–32], respectively. $\mathbf{B}$ is a static magnetic field and in our analysis we consider fields pointing along the three commonly used high symmetry directions of the lattice, namely, the [111], [100], and [110] directions. The parameters D and B wherever they appear as numerical values are quoted in units of J, which has the dimensions of energy. We develop the formalism below for a general spin quantum number S and present most numerical results for $S = 1$ and make comments about $S = 1/2$ at appropriate places.

In the absence of a magnetic field and the DMI term, the Hamiltonian with only a nearest neighbor exchange term has a macroscopically degenerate classical ground state and is a well known example of a classical spin liquid [33,34]. One set of states of this degenerate manifold are the ordered states of the all-in-all-out kind. A direct ($D > 0$) DMI term in the Hamiltonian selects this particular ordered state out of the degenerate manifold as the classical ground state, as noted in early work [35] and which can also be seen from a Luttinger-Tisza analysis [36]. Thus the classical ground state is one which has the translation invariance of the underlying fcc lattice.

Measurements and characterization of pyrochlore materials often involve applying a magnetic field along high symmetry directions of the lattice. We analyzed the renormalized spectra for fields of various strengths applied along three of the commonly utilized high symmetry directions of this lattice, namely, the [111], [100], and [110] directions shown in Fig. 1(b). In the presence of a magnetic field, the classical ground state naturally differs from the AIAO state at zero field. Using numerical minimization within the space of states in which spins belonging to a particular sublattice have the same orientation, we find the classical ground states for finite fields. We study fields pointing along one of the three high symmetry directions mentioned above. As expected on general grounds we find that for finite fields the moments tilt towards the field direction by a magnitude depending on the strength of the field. While the qualitative effect of the moments canting towards the field is similar for fields in all the three high symmetry directions, the details of how the moments tilt can depend on the direction of the field. For the [111] direction one of the moments is already aligned with the field and the other three moments tilt by the same angle towards the field as shown in Fig. 1(c). The canting happens in this case in such a manner that each spin rotates towards the field in a plane defined by its initial direction and the field direction. For the fields in the [100] direction too, this property holds. However, the magnitude of tilt is not the same for all the spins; one pair of sublattices have one tilt value and another pair have a different tilt value. Finally, for the [110] direction, the tilt towards the field is not in general in the plane defined by the initial moment direction and the field direction. For the field strengths that we have investigated, the tilting effect of a magnetic field on the classical ground state is small, as depicted for a representative case in Fig. 1(c). It shows the moments of the tetrahedral unit in the classical ground state without and with a magnetic field (of strength $B = 2.0J$) for $D = 0.1J$. Even though we have only analyzed field strengths far from saturation it might be of interest to the reader to have an estimate of the saturation fields. For the case of the field in the [111] direction, the energy function to be minimized can be written in an analytical form as a function of the tilt angle. In the Appendix, we present that function, and under certain stated assumptions, present how the canting angle changes with the field up to saturation. We emphasize again, however, that the data presented in the rest of main text are for fields far away from saturation.

Before we discuss our results for the renormalized spectra of the AIAO phase, we present below the relevant aspects of the formalism of LSWT and magnon interactions in general terms, in the notation that we use throughout the text.

We assume the spin model to be defined on a lattice which is a Bravais lattice with a number of sublattices. The classical ground state phases we consider are such that each spin belonging to a sublattice has a fixed orientation. Using a suitable rotation of axes we orient the local "z axis" (denoted using the superscript 3 below) along the direction of the moment at each

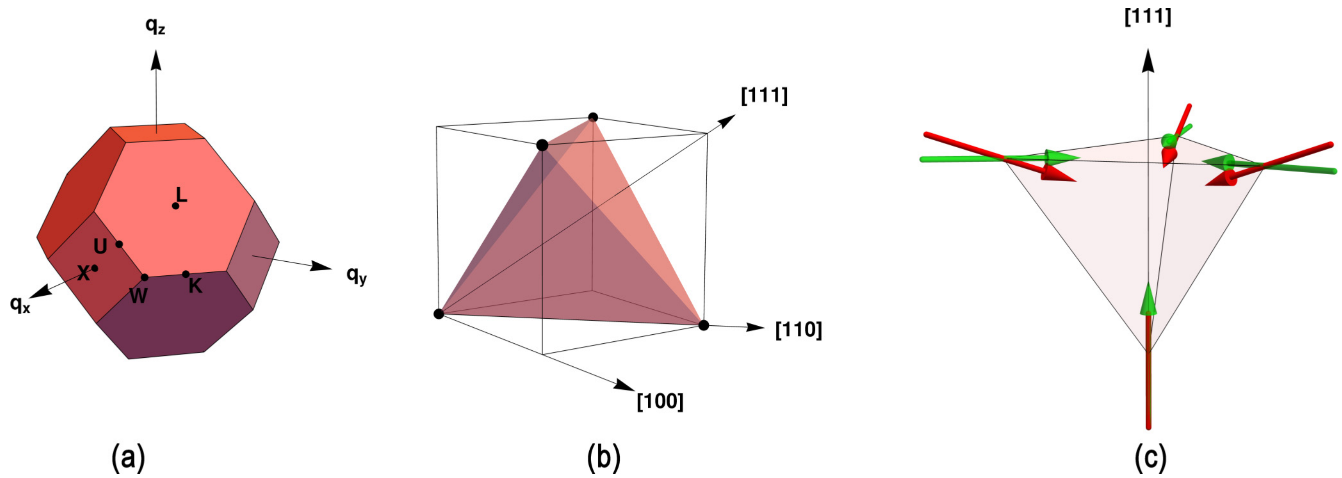

FIG. 1. (a) The Brillouin zone of the pyrochlore lattice with the locations of the high symmetry points used in this work. (b) The three high symmetry directions along which magnetic fields have been considered. (c) The classical ground states in the absence and the presence of a magnetic field. The red colored arrows are spin directions in the all-in-all-out phase which is the ground state in the absence of a field for a finite $D(=0.1J$ here). The green colored arrows are after a finite field ($B=2.0J$) is applied. The field is along the [111] direction in this example.

sublattice. The Hamiltonian H of Eq. (1) can be written as

$$\begin{aligned} H = \sum_{i\alpha, j\beta} & \big[J^{33}_{i\alpha;j\beta} S^3_{i\alpha} S^3_{j\beta} + J^{++}_{i\alpha;j\beta} S^+_{i\alpha} S^+_{j\beta} + J^{--}_{i\alpha;j\beta} S^-_{i\alpha} S^-_{j\beta} \\ & + J^{+-}_{i\alpha;j\beta} S^+_{i\alpha} S^-_{j\beta} + J^{-+}_{i\alpha;j\beta} S^-_{i\alpha} S^+_{j\beta} + J^{+3}_{i\alpha;j\beta} S^+_{i\alpha} S^3_{j\beta} \\ & + J^{3+}_{i\alpha;j\beta} S^3_{i\alpha} S^+_{j\beta} + J^{-3}_{i\alpha;j\beta} S^-_{i\alpha} S^3_{j\beta} + J^{3-}_{i\alpha;j\beta} S^3_{i\alpha} S^-_{j\beta}\big] \\ & - \sum_{i\alpha} B^3_\alpha S^3_{i\alpha} - \frac{1}{2} \sum_{i\alpha} (B^-_\alpha S^+_{i\alpha} + B^+_\alpha S^-_{i\alpha}). \end{aligned} \tag{2}$$

The sums over $i\alpha,\ j\beta$ above are unrestricted and run over all sites of the lattice. All coupling constants of the form $J^{[][]}_{i\alpha;j\beta}$ have the translation invariance of the underlying Bravais lattice and periodic boundary conditions are assumed when finite lattices are studied. We define the local axes unit vectors for every sublattice α : $(\hat{\mathbf{e}}^1_\alpha,\ \hat{\mathbf{e}}^2_\alpha,\ \hat{\mathbf{e}}^3_\alpha)$, with the moment pointing along $\hat{\mathbf{e}}^3_\alpha$ in the classical ground state. If the orientation of the sublattice α is given by the $(\theta_\alpha, \phi_\alpha)$ point on the unit sphere then we choose $(\hat{\mathbf{e}}^1_\alpha,\ \hat{\mathbf{e}}^2_\alpha,\ \hat{\mathbf{e}}^3_\alpha) = (\hat{\theta}_\alpha,\ \hat{\phi}_\alpha,\ \hat{r}_\alpha)$. $(\hat{\mathbf{e}}^1_\alpha,\ \hat{\mathbf{e}}^2_\alpha,\ \hat{\mathbf{e}}^3_\alpha)$ define a local right-handed coordinate system for each sublattice α, so we have $S^m_{i\alpha} = \mathbf{S}_{i\alpha} \cdot \hat{\mathbf{e}}^m_\alpha$ and $S^\pm_{i\alpha} = S^1_{i\alpha} \pm S^2_{i\alpha}$ and thus $S^m_{i\alpha}$ follow the standard spin commutation relations. In the last set of terms in Eq. (2) the scalar product $\mathbf{B} \cdot \mathbf{S}$ has been written using the components of B^m_α and $S^m_{i\alpha}$ along the local axes at the location of each spin with $B^\pm_\alpha \equiv (B^1_\alpha \pm iB^2_\alpha)$. As indicated above $B^3_\alpha, S^3_{i\alpha}$ are the components along the direction of the spin in the classical ground state.

We provide one example to make clear for the reader the relation between the terms in Eqs. (1) and (2). We consider, for illustration, the terms in Eq. (1) with the sublattice indices $\alpha = 1, \beta = 2$. $(\hat{\mathbf{e}}^1_1,\ \hat{\mathbf{e}}^2_1,\ \hat{\mathbf{e}}^3_1)$ are the orthonormal unit vectors of the local right-handed coordinate system associated with sublattice 1. The vector operator for the spin at sublattice 1 can be written as $\mathbf{S}_{i1} = \sum_m S^m_{i1}\ \hat{\mathbf{e}}^m_1$. The notation for $\mathbf{S}_{i2}$ is defined analogously. We note that $\hat{\mathbf{e}}^m_\alpha$ do not have a Bravais lattice site index, consistent with the fact that the studied classical ground state has the translation invariance of the underlying Bravais lattice. We reexpress the exchange and DMI terms corresponding to this pair, as follows:

$$\begin{aligned} & \frac{1}{2}[J\mathbf{S}_{i1} \cdot \mathbf{S}_{j2} + \mathbf{D}_{i1,j2} \cdot (\mathbf{S}_{i1} \times \mathbf{S}_{j2})] \\ & = \frac{1}{2}\left[\sum_{m,n} \big[J\hat{\mathbf{e}}^m_1 \cdot \hat{\mathbf{e}}^n_2 + \mathbf{D}_{i1,j2} \cdot \big(\hat{\mathbf{e}}^m_1 \times \hat{\mathbf{e}}^n_2\big)\big] S^m_{i1} S^n_{j2}\right] \\ & = \sum_{m,n} \mathcal{D}^{mn}_{i1;j2} S^m_{i1} S^n_{j2}. \end{aligned} \tag{3}$$

The factor of $\frac{1}{2}$ has been introduced to account for the fact that the sums in Eq. (2) are unrestricted. In writing the above we have assumed that $(i1,\ j2)$ are nearest neighbors. Given the unrestricted nature of the sums in Eq. (2), if $(i\alpha,\ j\beta)$ are not a nearest neighbor pair, $\mathcal{D}^{mn}_{i\alpha;j\beta}$ are zero for our Hamiltonian. We can now rewrite all the terms in the above expression in terms of $S^3_{i\alpha}, S^\pm_{i\alpha} = S^1_{i\alpha} \pm iS^2_{i\alpha}$. Doing so and collecting the coefficients appropriately yields Eq. (2). For instance, $J^{++}_{i1;j2}$ is given by

$$J^{++}_{i1;j2} = \tfrac{1}{4}\big[\mathcal{D}^{11}_{i1;j2} - i\mathcal{D}^{12}_{i1;j2} - i\mathcal{D}^{21}_{i1;j2} - \mathcal{D}^{22}_{i1;j2}\big]. \tag{4}$$

Equations (3) and (4) (and analogous ones for other sublattice pairs) establish the connection between the bare coupling constants, the classical ground state about which spin wave excitations are calculated, and the coupling constants in Eq. (2). Though we chose our nearest neighbor example to illustrate the relation, the notation of course is general and can incorporate broadly defined Hamiltonians with terms that are quadratic in spin operators (including generic single site anisotropy terms). The local axes conventions that we have used and the detailed expressions of all the coefficients $J^{[][]}_{i\alpha;j\beta}$ in terms of $\mathcal{D}^{mn}_{i\alpha;j\beta}$ following the same procedure outlined above can be found in the Appendix of earlier work by two of us [29], where our notation was introduced.

We use the Holstein-Primakoff (HP) [37] bosonic representation for the spin operators ($S^3_{i\alpha} = S - b^\dagger_{i\alpha} b_{i\alpha},\ \ S^+_{i\alpha} = \sqrt{2S - b^\dagger_{i\alpha} b_{i\alpha}}\ b_{i\alpha}$). The Hamiltonian equation (2) expressed in terms of $b_{i\alpha}$, retaining the leading order terms involving interactions among (HP) bosons, has the following structure:

$$H \approx H_{\rm SW} = H_{\rm LSWT} + H_{\rm int}, H_{\rm LSWT} = \mathcal{E}_{\rm GS}^{\rm LSWT} + \sum_{\mathbf{q},\alpha}[\epsilon_{\mathbf{q}\alpha} f^\dagger_{\mathbf{q}\alpha} f_{\mathbf{q}\alpha}] \tag{5}$$

$$\begin{aligned}
H_{\rm int} &= H_{\rm int}^{33} + H_{\rm int}^{++} + H_{\rm int}^{--} + H_{\rm int}^{+-} + H_{\rm int}^{-+} + H_{\rm int}^{3+} + H_{\rm int}^{+3} + H_{\rm int}^{3-} + H_{\rm int}^{-3}, \quad \text{where}\\
H_{\rm int}^{33} &= \frac{1}{N}\sum_{\substack{\{\mathbf{q_i}\},\mathbf{Q}\\ \alpha,\beta}} \tilde{J}^{33}_{\alpha\beta}(\mathbf{Q}) b^\dagger_{\mathbf{q_1}\alpha} b_{\mathbf{q_1}+\mathbf{Q}\alpha} b^\dagger_{\mathbf{q_3}\beta} b_{\mathbf{q_3}-\mathbf{Q}\beta},\\
H_{\rm int}^{++} &= -\frac{1}{2N}\sum_{\substack{\{\mathbf{q_i}\}\\ \alpha,\beta}} \tilde{J}^{++}_{\alpha\beta}(\mathbf{q_2}) b_{\mathbf{q_2}\alpha} b^\dagger_{\mathbf{q_2}+\mathbf{q_3}+\mathbf{q_4}\beta} b_{\mathbf{q_3}\beta} b_{\mathbf{q_4}\beta} - \frac{1}{2N}\sum_{\substack{\{\mathbf{q_i}\}\\ \alpha,\beta}} \tilde{J}^{++}_{\alpha\beta}(-\mathbf{q_4}) b^\dagger_{\mathbf{q_2}+\mathbf{q_3}+\mathbf{q_4}\alpha} b_{\mathbf{q_2}\alpha} b_{\mathbf{q_3}\alpha} b_{\mathbf{q_4}\beta},\\
H_{\rm int}^{+-} &= -\frac{1}{2N}\sum_{\substack{\{\mathbf{q_i}\}\\ \alpha,\beta}} \tilde{J}^{+-}_{\alpha\beta}(\mathbf{q_2}+\mathbf{q_3}-\mathbf{q_4}) b_{\mathbf{q_2}+\mathbf{q_3}-\mathbf{q_4}\alpha} b^\dagger_{\mathbf{q_2}\beta} b^\dagger_{\mathbf{q_3}\beta} b_{\mathbf{q_4}\beta} - \frac{1}{2N}\sum_{\substack{\{\mathbf{q_i}\}\\ \alpha,\beta}} \tilde{J}^{+-}_{\alpha\beta}(\mathbf{q_2}+\mathbf{q_3}-\mathbf{q_4}) b^\dagger_{\mathbf{q_4}\alpha} b_{\mathbf{q_2}\alpha} b_{\mathbf{q_3}\alpha} b^\dagger_{\mathbf{q_2}+\mathbf{q_3}-\mathbf{q_4}\beta},\\
H_{\rm int}^{3+} &= -\sqrt{\frac{2S}{N}}\sum_{\substack{\{\mathbf{q_i}\}\\ \alpha,\beta}} \tilde{J}^{3+}_{\alpha\beta}(-\mathbf{q_3}) b^\dagger_{\mathbf{q_2}+\mathbf{q_3}\alpha} b_{\mathbf{q_2}\alpha} b_{\mathbf{q_3}\beta} - \sqrt{\frac{S}{8N}}\sum_{\substack{\{\mathbf{q_i}\}\\ \alpha,\beta}} \tilde{J}^{3+}_{\alpha\beta}(\mathbf{0}) b^\dagger_{\mathbf{q_2}+\mathbf{q_3}\beta} b_{\mathbf{q_2}\beta} b_{\mathbf{q_3}\beta},\\
H_{\rm int}^{+3} &= -\sqrt{\frac{2S}{N}}\sum_{\substack{\{\mathbf{q_i}\}\\ \alpha,\beta}} \tilde{J}^{+3}_{\alpha\beta}(\mathbf{q_2}-\mathbf{q_3}) b_{\mathbf{q_2}-\mathbf{q_3}\alpha} b^\dagger_{\mathbf{q_2}\beta} b_{\mathbf{q_3}\beta} - \sqrt{\frac{S}{8N}}\sum_{\substack{\{\mathbf{q_i}\}\\ \alpha,\beta}} \tilde{J}^{+3}_{\alpha\beta}(\mathbf{0}) b^\dagger_{\mathbf{q_2}+\mathbf{q_3}\alpha} b_{\mathbf{q_2}\alpha} b_{\mathbf{q_3}\alpha},
\end{aligned} \tag{6}$$

where the other terms ($H_{\rm int}^{--}$, $H_{\rm int}^{-+}$, $H_{\rm int}^{3-}$, $H_{\rm int}^{-3}$) in Eq. (6) are related to the terms written above because of the Hermiticity of the Hamiltonian. In the terms that we have written in Eq. (6), though the magnetic field is not seen explicitly it is included: the LSWT spectra $\epsilon_{\mathbf{q}\alpha}$ depend on it explicitly and the coupling constants depend on it implicitly since the field plays a role in determining the classical ground state and the various coupling constants [see the discussion leading to Eqs. (3) and (4)].

The noninteracting part of the Hamiltonian $H_{\rm LSWT}$ is written in terms of new bosonic operators $\{f_{\mathbf{q}\alpha}\}([f_{\mathbf{q}\alpha}, f^\dagger_{\mathbf{q}'\alpha'}] = \delta_{qq'}\delta_{\alpha\alpha'})$ and $\epsilon_{\mathbf{q}\alpha}$ are the spin wave energies at the level of noninteracting magnons. We denote by $\mathbf{\Gamma_q}$ the linear transformation relating the old and the new bosonic operators, $[\mathbf{f_q}\ \mathbf{f}^\dagger_{-\mathbf{q}}]^T = \mathbf{\Gamma_q}[\mathbf{b_q}\ \mathbf{b}^\dagger_{-\mathbf{q}}]^T$. For the construction of $\mathbf{\Gamma_q}$ we follow a well established procedure [38]. In the presence of a finite magnetic field we determine the classical ground state, necessary to proceed with the spin wave analysis, using numerical optimization. The evaluation of $\epsilon_{q\alpha}$ includes the effect of a finite magnetic field term. We note that the field term also results in terms which are linear in the transverse spin components but such terms (in conjunction with similar terms from the exchange terms) vanish for a valid extremum of the classical energy function.

$H_{\rm int}$ is the magnon-magnon interaction part of the Hamiltonian, obtained by keeping the next order terms beyond those required for linear spin wave theory using Holstein-Primakoff bosons. We retain terms until S^0 in writing $H_{\rm int}$ and consider leading order effects of nonlinear spin wave theory (NLSWT).

We consider the time-ordered Green's function at zero temperature:

$$i\mathbf{G}_{\alpha\beta}(q, t_1 - t_2) = \frac{\langle \mathbf{\Psi}_{\rm GS}|\mathcal{T}(f_{q\alpha}(t_1) f^\dagger_{q\beta}(t_2))|\mathbf{\Psi}_{\rm GS}\rangle}{\langle \mathbf{\Psi}_{\rm GS}|\mathbf{\Psi}_{\rm GS}\rangle}. \tag{7}$$

Here $|\mathbf{\Psi}_{\rm GS}\rangle$ is the ground state of $H_{\rm SW}$ in Eq. (5) and $f_{q\alpha}(t_1)$ and $f^\dagger_{q\beta}(t_2)$ are operators in the Heisenberg representation. $\mathcal{T}$ is the time-ordering operator which orders operators from latest to earliest times and $i \equiv \sqrt{-1}$. Following the standard formulation for such Green's functions [39] we have

$$\begin{aligned}
&i\mathbf{G}_{\alpha\beta}(q, t_1 - t_2)\\
&\quad = \frac{{}_f\langle \mathbf{0}|\mathcal{T}\big[\hat{f}_{q\alpha}(t_1)\hat{f}^\dagger_{q\beta}(t_2)\exp\big(-i\int_{-\infty}^{\infty}\hat{H}_{\rm int}(t)dt\big)\big]|\mathbf{0}\rangle_f}{{}_f\langle \mathbf{0}|\mathcal{T}\exp\big(-i\int_{-\infty}^{\infty}\hat{H}_{\rm int}(t)dt\big)|\mathbf{0}\rangle_f}.
\end{aligned} \tag{8}$$

The "^" above the operators indicates the interaction picture with the noninteracting Hamiltonian being $H_{\rm LSWT}$. $H_{\rm int}$ has already been defined in Eq. (6). $|\mathbf{0}\rangle_f$ is the vacuum state of the f bosons ($f_{\mathbf{q}\alpha}|\mathbf{0}\rangle_f = 0, \forall\{q,\alpha\}$) or, equivalently, the ground state of $H_{\rm LSWT}$. $\mathbf{G}_{\alpha\beta}(q,\omega) = \int \mathbf{G}_{\alpha\beta}(q,t)\exp(i\omega t)dt$ satisfies the Dyson equation:

$$\begin{aligned}
\mathbf{G}_{\alpha\beta}(q,\omega) &= \left[\frac{1}{\mathbf{G}_0^{-1}(q,\omega) - \mathbf{\Sigma}(q,\omega)}\right]_{\alpha\beta}, \ \text{where}\\
[\mathbf{G}_0]_{\alpha\beta}(q,\omega) &= \left[\frac{1}{\omega - \epsilon_{q\alpha} + i\eta}\right]\delta_{\alpha\beta},
\end{aligned} \tag{9}$$

where $\mathbf{\Sigma}(q,\omega)$ is the irreducible self-energy. The poles of the Green's function $\mathbf{G}_{\alpha\beta}(q,\omega)$ determine the renormalized spectra and their widths. In this work we calculate the leading order term of the irreducible self-energy $\mathbf{\Sigma}(q,\omega)$ and evaluate the poles of the Green's function to obtain the renormalized spectra.

We note here the $H_{\rm int}$ as written in Eq. (6) is not normal ordered when expressed in terms of the f bosons, in terms of which the vacuum of the noninteracting Hamiltonian is defined. In order to evaluate the first term in self-energy using the application of Wick's theorem, we use the prescribed method of normal ordering the operators of the interaction

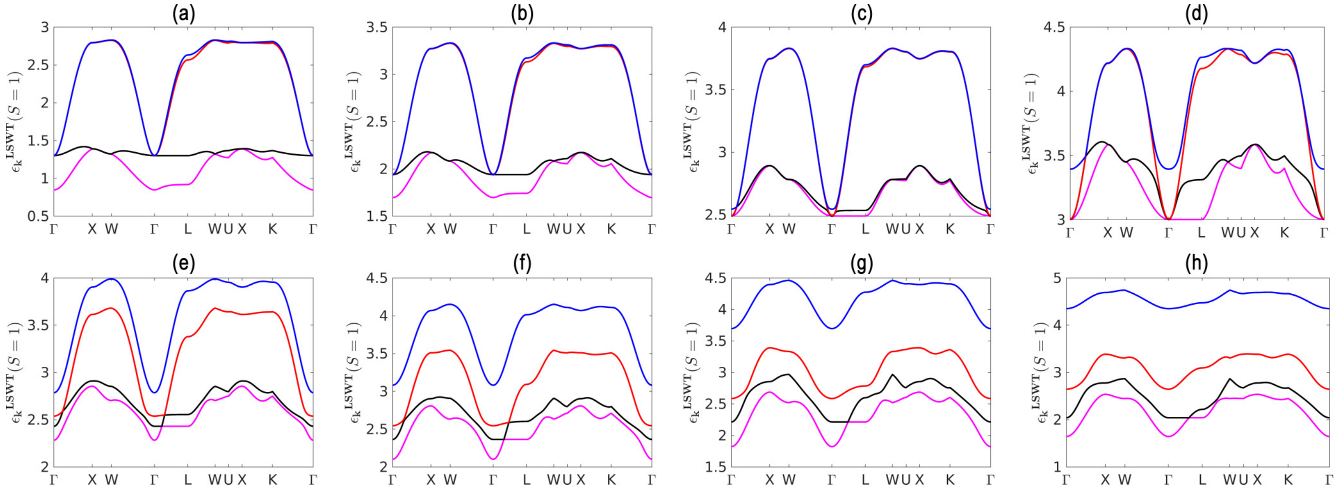

FIG. 2. A representative selection of linear spin wave theory (LSWT) spectra. (a)–(d) Magnon bands of the LSWT Hamiltonian for $D = 0.1J,\ 0.2J,\ 0.3J,\ 0.4J$ and $B \approx 0 (= 0.005J)$. (e)–(h) Magnon bands of the LSWT Hamiltonian for $D = 0.3J$ and $B = 0.5J,\ 1.0J,\ 2.0J,\ 3.0J$ along the [111] direction. The interacting spin wave analysis discussed in the rest of this work studies the leading order corrections to LSWT results for $D \in (0.1J,\ 0.2J,\ 0.3J,\ 0.4J,\ 0.5J)$ and $B \in (0.5J,\ 1.0J,\ 2.0J,\ 3.0J)$ along the [111], [100], and [110] directions.

Hamiltonian which appear with the same time label [40], before applying the contractions.

Though the procedure is known, we provide here one illustrative example of how the contributions to the leading order self-energy are evaluated for our case, in our notation.

Consider one of the terms of the interaction Hamiltonian, namely, H_{int}^{33}, which when written in terms of the f bosons has the following form:

$$
\begin{aligned}
H_{\mathrm{int}}^{33} &= \frac{1}{N} \sum_{\substack{\{\mathbf{q_i}\},\mathbf{Q}\\ \alpha,\beta}} \tilde{J}^{33}_{\alpha\beta}(\mathbf{Q}) b^{\dagger}_{\mathbf{q_1}\alpha} b_{\mathbf{q_1+Q}\alpha} b^{\dagger}_{\mathbf{q_3}\beta} b_{\mathbf{q_3-Q}\beta} \\
&= \frac{1}{N} \sum_{\substack{\{\mathbf{q_i}\},\mathbf{Q}\\ \alpha,\beta,\{\beta_i\}}} \tilde{J}^{33}_{\alpha\beta}(\mathbf{Q}) \\
&\quad \times \big[[\mathbf{\Gamma}^{-1}(\mathbf{q}_1)]^*_{\alpha,4+\beta_1} f_{-\mathbf{q}_1\beta_1} + [\mathbf{\Gamma}^{-1}(\mathbf{q}_1)]^*_{\alpha,\beta_1} f^{\dagger}_{\mathbf{q}_1\beta_1}\big] \\
&\quad \times \big[[\mathbf{\Gamma}^{-1}(\tilde{\mathbf{q}}_1)]_{\alpha,\beta_2} f_{\tilde{\mathbf{q}}_1,\beta_2} + [\mathbf{\Gamma}^{-1}(\tilde{\mathbf{q}}_1)]_{\alpha,4+\beta_2} f^{\dagger}_{-\tilde{\mathbf{q}}_1,\beta_2}\big] \\
&\quad \times \big[[\mathbf{\Gamma}^{-1}(\mathbf{q}_3)]^*_{\beta,4+\beta_3} f_{-\mathbf{q}_3\beta_3} + [\mathbf{\Gamma}^{-1}(\mathbf{q}_3)]^*_{\beta,\beta_3} f^{\dagger}_{\mathbf{q}_3\beta_3}\big] \\
&\quad \times \big[[\mathbf{\Gamma}^{-1}(\tilde{\mathbf{q}}_3)]_{\beta,\beta_4} f_{\tilde{\mathbf{q}}_3,\beta_4} + [\mathbf{\Gamma}^{-1}(\tilde{\mathbf{q}}_3)]_{\beta,4+\beta_4} f^{\dagger}_{-\tilde{\mathbf{q}}_3,\beta_4}\big], \\
&\qquad \text{where } \tilde{\mathbf{q}}_1 = \mathbf{q}_1 + \mathbf{Q} \text{ and } \tilde{\mathbf{q}}_3 = \mathbf{q}_3 - \mathbf{Q}.
\end{aligned} \tag{10}
$$

Every quartic term in Eq. (10) which has two creation and annihilation operators can in principle contribute a nonvanishing term to the first order self-energy. One such term has the form $f^{\dagger}_{\mathbf{q}_1\beta_1} f_{\mathbf{q}_1+\mathbf{Q},\beta_2} f^{\dagger}_{\mathbf{q}_3\beta_3} f_{\mathbf{q}_3-\mathbf{Q},\beta_4}$. Writing this term in normal ordered form and applying Wick's theorem will result in a contribution to the first order self-energy from this term, which we call $\mathbf{\Sigma}^{1010,33}_{\mu\nu}(q,\omega)$ (where $1 \Rightarrow$ creation operator, $0 \Rightarrow$ annihilation operator), of the following form:

$$
\begin{aligned}
\mathbf{\Sigma}^{1010,33}_{\mu\nu}(\mathbf{q},\omega) &= \frac{1}{N} \sum_{\substack{\mathbf{Q}\\ \alpha,\beta,\beta_3}} \tilde{J}^{33}_{\alpha\beta}(\mathbf{Q}) [\mathbf{\Gamma}^{-1}(\mathbf{q})]^*_{\alpha,\mu} [\mathbf{\Gamma}^{-1}(\mathbf{q}+\mathbf{Q})]_{\alpha,\beta_3} \\
&\quad \times [\mathbf{\Gamma}^{-1}(\mathbf{q}+\mathbf{Q})]^*_{\beta,\beta_3} [\mathbf{\Gamma}^{-1}(\mathbf{q})]_{\beta,\nu}.
\end{aligned} \tag{11}
$$

There will clearly be several more contributions like this to the self-energy from H_{int}^{33}. The total irreducible self-energy at first order, which we use for evaluation of renormalized magnon bands in the rest of this work, is the sum of such contributions from all the quartic terms in Eq. (6). We note that at this order the self-energy is frequency independent and Hermitian. We emphasize that the notation we have used here is completely general and the above formalism is applicable for the analysis of renormalized magnon spectra of an ordered phase of a lattice with a basis, provided the spin wave analysis is about a classical ground state which has the translation invariance of the underlying Bravais lattice. We now present our results of this analysis for the AIAO phase of the pyrochlore lattice described by Eq. (1).

III. RENORMALIZED MAGNON SPECTRA

For the evaluation of the renormalized spectra of the Hamiltonian we have used system sizes of $4N^3$ sites with $N = 10, 20$. For magnon spectra along a high symmetry path the evaluation of the leading order self-energy involves a sum over momenta over the Brillouin zone. We evaluate that sum for the lattice sizes mentioned above and have verified that the difference in the final depicted spectra, a measure of finite size errors, is small. Throughout the text we show spectra along a path passing through high symmetry points in the Brillouin zone. Figure 1(a) depicts the Brillouin zone and the high symmetry points.

Before we discuss the renormalized spectra it is useful to have for reference LSWT spectra for different D and B values. Figure 2 shows the magnonic band structure of the LSWT Hamiltonian for a vanishingly small magnetic field for $D = 0.1J,\ 0.2J,\ 0.3J,$ and $0.4J$ (top row). We recall that an evaluation of the magnon bands of the all-in-all-out state in the absence of the DMI results in two sets of doubly degenerate bands, one flat band at zero energy and another dispersive [41]. The DMI results in a gap as can be seen in

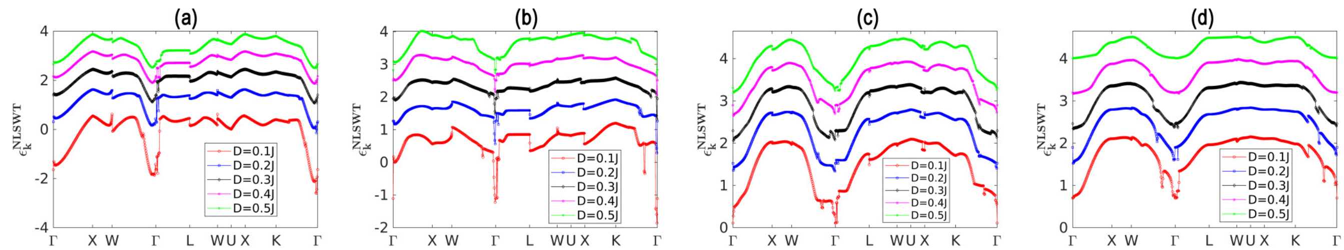

FIG. 3. (a)–(d) The renormalized spectrum for the four bands, from the lowest to the highest, evaluated using the self-energy at first order in nonlinear spin wave theory for $B \approx 0 (= 0.005J)$, $S = 1$ and several strengths of the DMI interaction. For reference, the corresponding linear spin wave theory bands can be found in Fig. 2.

Fig. 2 and also makes the lower bands dispersive. We now investigate here what happens to these spectra under spin wave interactions.

At the level of first order in spin wave interactions the spectra are simply renormalized but remain sharp. This follows from the frequency independence and the Hermiticity of the evaluated first order self-energy matrices over the Brillouin zone. At this leading order in magnon interactions we find significant renormalization of the LSWT spectra. Figures 3(a)–3(d) depict the renormalized bands starting from the lowest to the highest for values of DMI in the range $D \in [0.1J, 0.5J]$. The general effect of the energy of the bands increasing as the value of DMI is increased remains true for the renormalized bands, however, with substantial renormalization. We also find that the spectra in the vicinity of the Γ point get renormalized to negative values for the lowest band indicating an instability of the AIAO phase to spin wave interactions. The data shown in Fig. 3 are depicted for $S = 1$. We have also studied the Hamiltonian for $S = 1/2$. The linear spin wave spectra are a simple linear function of the spin quantum number in the absence of a field. Hence all the magnon energies simply get renormalized to half their values in Fig. 2 (top row). This results in the lowest band being nearer to the degenerate classical spin liquid manifold for $S = 1/2$ than for $S = 1$. Broadly, we find that this results in the increased fragility of the AIAO phase for $S = 1/2$ compared to $S = 1$. The instability indicated by the negative values of the renormalized spectra are seen to be present for higher values of D in the case of $S = 1/2$ compared to $S = 1$. We note here that a tiny field of strength $0.005J$ was added to induce a small breaking of exact degeneracy in bands (which exists for $B = 0$) and thence permit unambiguous band labels in the noninteracting Green's function. This also enables us to clearly identify bands with labels during the evaluation of the self-energy, which involves a sum over the Brillouin zone wave vectors and bands. The data presented in Fig. 3 are for a lattice of $4N^3$, $N = 20$ spins.

In Sec. II we described the effect of magnetic fields on the classical ground state. We now present our results on the spectral renormalization because of magnetic fields along the three high symmetry directions. We have studied field strengths of $B = 0.5J$, $1.0J$, $2.0J$, $3.0J$ for the all strengths of DMI we have analyzed until now. These fields are considerably smaller than the expected saturation fields for the DMI strengths studied (see the Appendix). For reference, a selection of noninteracting magnon spectra have been presented in Figs. 2(e)–2(h).

Figure 4 depicts representative data showing the effects of a magnetic field. The top row depicts the LSWT spectra for $D = 0.3J$ and $B = 2.0J$, for $\mathbf{B} \parallel [111], [100],$ and $[110]$, respectively. The bottom row depicts the renormalized spectra for the lowest band for various values of the strength of the DMI. A comparison between the plots in the bottom row and those of Fig. 3 clearly indicates that between the DMI and the field the former is the more important factor in determining the extent of the renormalization for the parameter ranges that we have studied. In both Figs. 3 and 4 we notice the appearance of several discontinuities and singularities in the renormalized spectrum. We find these features under one or more of several conditions. They often occur at high symmetry points and most prominently near the Γ point. These discontinuities appear to have a regular trend in the vicinity of those points, in the sense that the bands have a continuous behavior in either direction of the high symmetry point along the path. These indicate a discontinuous approach towards the high symmetry point from different directions in the Brillouin zone, within our evaluation method. A related kind of singular behavior happens to be at those wave vectors in the Brillouin zone where the LSWT spectra have point degeneracies. In LSWT these are usually avoided crossings with very small gaps for the lattice sizes we study. Sometimes finite discontinuities like these can also be found in regions of the Brillouin zone not necessarily close to any high symmetry point or small gaps in the LSWT spectra [see, for instance, the segment $K\Gamma$ in Fig. 4(f)]. Considering the proximity of such singular behavior in several cases to points in the Brillouin zone with small gaps, we believe many such jumps are the results of using the perturbative evaluation of the self-energy beyond the limits of its applicability. In the absence of such problems caused in a perturbative evaluation by small gaps in multiband systems these kinds of discontinuities have been reported in studies of magnon interactions in Bravais lattices, for instance, in the triangular lattice [7]. There they were found to be regions with an enhanced scattering rate for magnons. The fact that these features in the spectra are likely associated with an enhanced scattering rate is also indicated by the fact that an increase in the strength of DMI reduces the size of these effects, as is clear in Figs. 4(d)–4(f). An increase in DMI takes the single magnon spectrum further away from the degenerate classical manifold at $D = 0$, thus reducing the available scattering space that is close to the band energy. It is likely that a nonperturbative evaluation of the self energy and/or a higher order calculation will result in regular behavior near such points. However, since these jumps are at isolated points

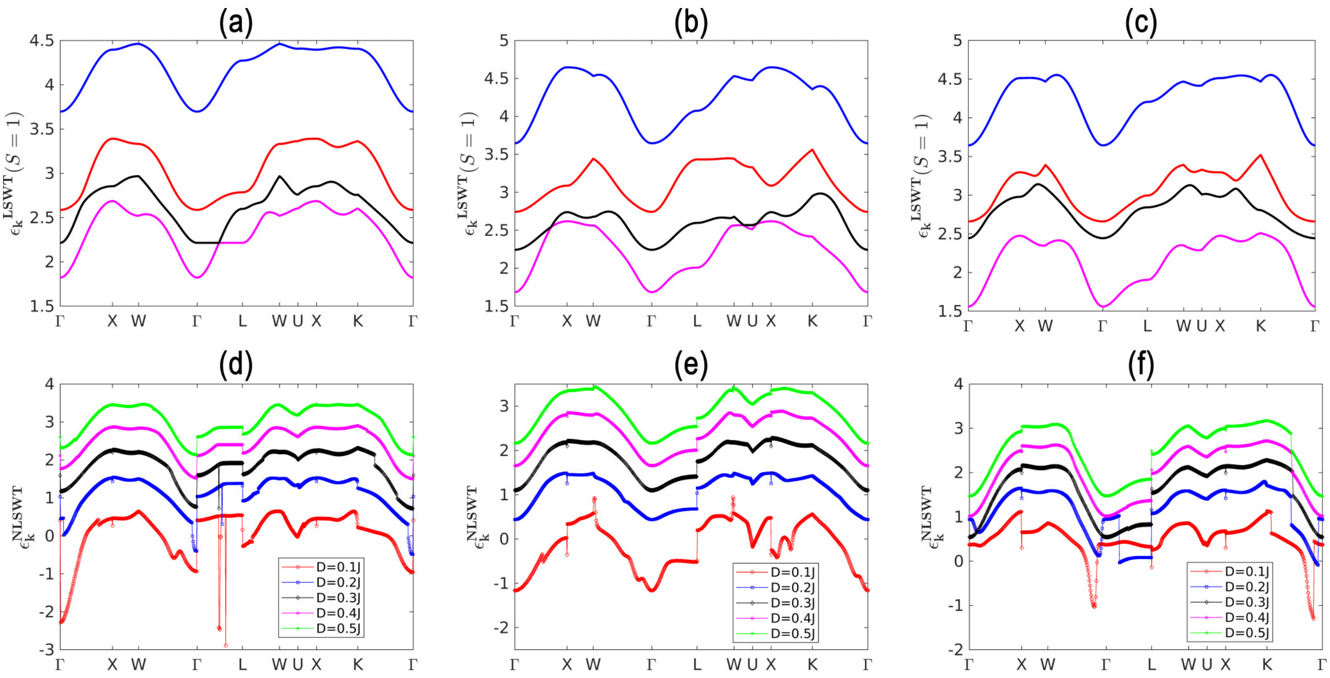

FIG. 4. Spectral renormalization with a magnetic field: (a)–(c) LSWT bands for a magnetic strength of $B = 2.0J$ and $D = 0.3J$ applied along the [111] (a), [100] (b), and [110] (c), directions. (d)–(f) The renormalized spectra for the lowest band for the same three directions for leading order spin wave interactions for $D \in [0.1J,\ 0.2J,\ 0.3J,\ 0.4J,\ 0.5J]$.

(in a three-dimensional Brillouin zone) they do not result in substantial loss in accuracy for data that we present later for quantities over the full zone. We have not explored in this work possible methods to regularize the data near such points, such as introducing small terms in the Hamiltonian to increase the gap at such degeneracies. We note, furthermore, that some of these point degeneracies are topological in nature and a proper treatment of interacting magnons around such points may not be possible using a perturbative framework.

As can be seen by a comparison of Figs. 3 and 4, for the lowest band we notice that presence of a magnetic field has renormalized the bands further down for all the values of D we have studied. It is relevant here to probe the effect on the renormalized spectra by varying the field strength and also investigate the effects on the other bands. Figure 5 presents both the noninteracting magnon spectra as well as the renormalized spin wave spectra for several different values of the magnetic field and for all four bands of the Hamiltonian. It is clear that for the lowest band the stronger renormalization towards lower values as the field strength is increased is generically true. Thus an increase in field strength for a given value of D increases the tendency towards destabilization of the phase. We have shown in Fig. 5 data for fields in the [111] direction but the above statement is true also for the other directions we have analyzed. The effect of the field, however, can depend on the band being considered. For instance, we see that the trend of decreasing renormalized spectra for an increasing field strength is reversed when we consider the highest band as can be seen in Fig. 5(h). The kind of nonanalytic behaviors discussed for the lowest band earlier are also present for the higher bands and, as in the case of the lowest band, the discontinuities decrease in magnitude as the strength of the DMI is increased.

Ground state energy and renormalized magnon spectra

In the previous section we have been discussing the extent of spectral renormalization because of magnon interactions along high symmetry paths in the Brillouin zone. We now analyze the effect of magnon interactions on the spectra over the whole zone. The obvious way to extract this is to probe a quantity which is dependent over all magnon frequencies. One such physical quantity with a simple dependence on magnon energies is the ground state energy. In the absence of magnon interactions we know that the ground state energy of the noninteracting Hamiltonian is given by

$$\mathcal{E}_{\rm GS}^{\rm LSWT} = \mathcal{E}_0 + {\sum_{\mathbf{q},\alpha}}' \eta_{\mathbf{q}} \epsilon^{\rm LSWT}_{-\mathbf{q}\alpha}, \tag{12}$$

where $\mathcal{E}_0 \equiv NS(S+1)\sum_{\alpha\beta} \tilde{J}^{33}_{\alpha\beta}(0) - N(S+\frac{1}{2})\sum_{\alpha} B^3_{\alpha}$ is a constant independent of the magnon frequencies. The "$\prime$" over the summation indicates that there is one term in the sum for each unique $(\mathbf{q}, -\mathbf{q})$ pair. $\eta_{\mathbf{q}}$ is 1 for all wave vectors in the zone except for those points for which $\mathbf{q}$ and $-\mathbf{q}$ differ by a reciprocal lattice vector, in which case $\eta_{\mathbf{q}} = \frac{1}{2}$. Under spectral renormalization, the renormalized spectra obtained from the poles of the Green's function are the single particle excitation energies of the interacting Hamiltonian. Replacing the noninteracting magnon energies in the above expression with the renormalized energies we can obtain, using the change in the evaluated ground state energy, an estimate of the effect of

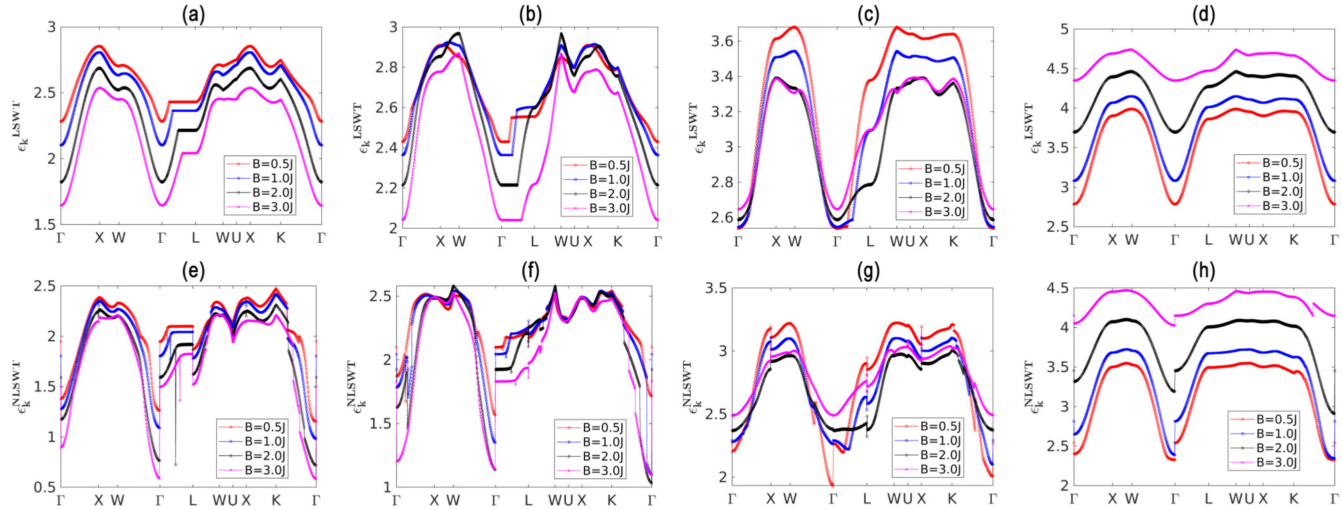

FIG. 5. Spectral renormalization of all bands as a function of the magnetic field: (a)–(d) LSWT bands (lowest to highest) for magnetic field strengths $B \in [0.5J,\ 1.0J,\ 2.0J,\ 3.0J]$ and $D = 0.3J$ applied along the [111] direction. (e)–(h) The renormalized spectra for leading order spin wave interactions for the same parameters as in the figures in the top row.

magnon interactions over the whole band. Thus

$$\mathcal{E}_{\mathrm{GS}}^{\mathrm{NLSWT}} = \mathcal{E}_0 + {\sum_{\mathbf{q},\alpha}}' \eta_{\mathbf{q}} \epsilon_{-\mathbf{q}\alpha}^{\mathrm{NLSWT}} \tag{13}$$

can be considered to be the estimate of the ground state energy in the presence of the interactions. Figure 6 depicts the relative change in the ground state energy estimates because of magnon interactions. Clearly, as expected from earlier plots, a higher value of D results in a smaller correction and hence a smaller overall effect of the interaction terms. Interestingly, though for a given value of D an increase in the strength of the magnetic field does increase the system's tendency to be unstable by renormalizing the lowest band to smaller values, overall for a bulk quantity like $\mathcal{E}_{\mathrm{GS}}$ the field seems to work against the spin wave interactions. For instance, in Fig. 6, at any given D increasing the value of the field is taking the $\mathcal{E}_{\mathrm{GS}}^{\mathrm{NLSWT}}$ value closer to $\mathcal{E}_{\mathrm{GS}}^{\mathrm{LSWT}}$, the value in the noninteracting limit. This essentially is a result of the fact that the field (unlike the DMI strength D) affects different bands differently and the bulk quantities being a sum over all bands feel the resulting cancellation effect.

IV. TWO-MAGNON CONTINUUM AND MAGNON DECAY

In the previous section we analyzed the poles of the single particle Green's function by evaluating the leading order term of the self-energy. At this order, as mentioned in the previous section, the poles are real and hence magnon interactions result only in the renormalization of the LSWT spectra while keeping the excitations sharp. The lowest order term which can result in poles with an imaginary part is at second order of terms involving the three bosons, for, e.g., $\tilde{J}_{\alpha\beta}^{3+}$, etc., in Eq. (6).

In principle, such a second order term can result in magnon decay via scattering into two magnons [8]. A detailed analysis of the pole structure and the associated imaginary parts requires the evaluation of the second order self-energy and a numerical search for the singularities of the Green's function using the evaluated self-energy until the second order. However, it is possible to obtain preliminary information about the

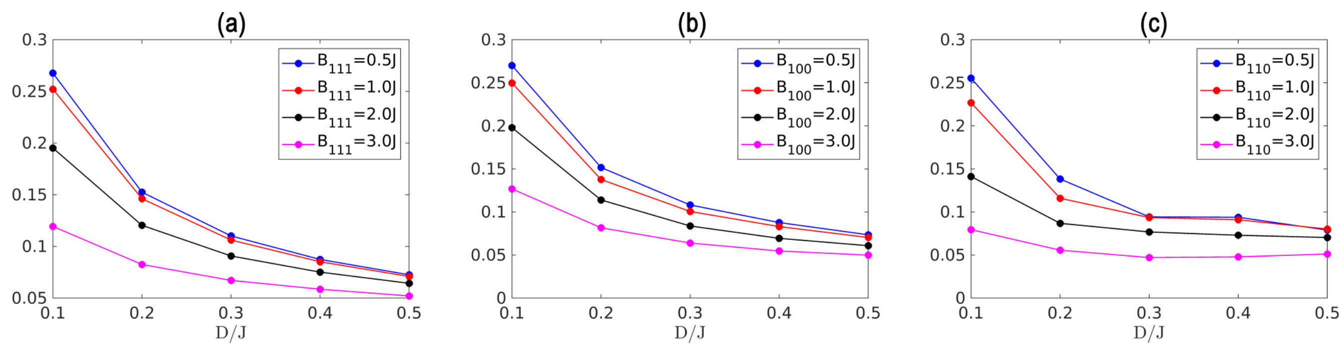

FIG. 6. The relative difference between the estimates of the ground state energy from linear and nonlinear spin wave theory, with magnetic fields along three high symmetry directions and for various D values. (a)–(c) The quantity plotted in all three panels is $\frac{\mathcal{E}_{\mathrm{GS}}^{\mathrm{LSWT}} - \mathcal{E}_{\mathrm{GS}}^{\mathrm{NLSWT}}}{|\mathcal{E}_{\mathrm{GS}}^{\mathrm{LSWT}}|}$, with magnetic field B along the [111], [100] and [110] directions respectively.

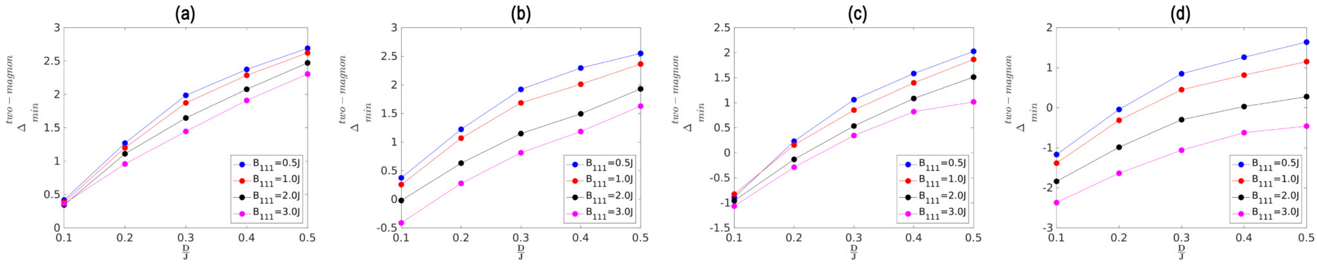

FIG. 7. The difference between the bottom of the two-magnon continuum at each wave vector and the band energy, minimized over the whole Brillouin zone and all decay channels. A negative value indicates that the condition [Eq. (14)] for the magnon decay is satisfied, for the band considered, somewhere in the Brillouin zone. Panels (a)–(d) are the data for the first (lowest), second, third, and fourth band, respectively. Data presented are evaluated for a lattice size of $4N^3 (N = 20)$ spins.

approximate energy regions where magnon decay is allowed using the second order self-energy at the LSWT energies. In that approximation in order for magnon decay to be possible the LSWT spectra have to satisfy certain kinematic conditions [8,42,43]. For instance, for the decay of the α-th band at the wave vector k into two magnons in the β-th and γ-th bands, requires

$$\epsilon_{\mathbf{k},\alpha} = \epsilon_{\mathbf{q},\beta} + \epsilon_{\mathbf{k}-\mathbf{q},\gamma} \tag{14}$$

for some $\mathbf{q}$ in the Brillouin zone. Thus there should be an intersection of the band of two-magnon excitations corresponding to a given momentum with the single magnon band at the same wave vector for such a decay to be possible. A specific triplet (α, β, γ) in Eq. (14) is a particular decay channel and a given band α can decay via multiple channels. We have investigated this possibility of decay for the system we are studying and the results are displayed in Fig. 7.

The quantity $\Delta_{\text{min}}^{\text{two-magnon}}$ which has been plotted is defined in the following manner:

$$\Delta_{\text{min}}^{\text{two-magnon}}(\alpha) = \min_{\mathbf{k},\mathbf{q},\beta,\gamma} [(\epsilon_{\mathbf{q},\beta} + \epsilon_{\mathbf{k}-\mathbf{q},\gamma}) - \epsilon_{\mathbf{k},\alpha}], \tag{15}$$

where $\mathbf{k}, \mathbf{q}$ are both vectors in the first Brillouin zone. Thus the $\Delta_{\text{min}}^{\text{two-magnon}}(\alpha)$ quantity is related to the gap between the bottom of the two-magnon continuum and the energy of the α-th band at wave vectors in the Brillouin zone. The minimization over (k, β, γ) indicates, should the minimum be a negative number, that the two-magnon continuum and the band intersect somewhere in the Brillouin zone. Thus Fig. 7 depicts a one-parameter diagnostic, for the ranges of B and D we have studied, to indicate if a magnon decay is possible.

The data clearly demonstrate that the lowest band, if it is not destabilized by the leading order interaction term, does not satisfy the kinematic condition for decay for the range of fields and DMI interactions that we have studied. Furthermore, we see clearly that the tendency to decay increases for any given strength of DMI with the increase of the strength of the magnetic field and decreases as the strength of the DMI is increased. We note here that the condition equation (14) is a necessary, but not a sufficient condition for magnon decay through this mechanism. A nonvanishing self energy matrix element will also require the relevant matrix element dependent on $\tilde{J}^{3+}_{\alpha\beta}$, etc., to be nonzero. Thus the results of Fig. 7 should be understood as being indicative of the parameters where the bands are protected against decay and possible parameter regions where decay might occur, provided other conditions are satisfied.

V. SUMMARY AND DISCUSSION

The all-in-all-out phase of the pyrochlore lattice is a very suitable platform for probing the effect of spin wave interactions. It is a noncollinear ground state, which can be close in parameter and energy space to a macroscopically degenerate ground state manifold of a geometrically frustrated system. In this preliminary analysis of the effect of spin wave interactions in this phase we have shown that the stability of the phase can be jeopardized below some strength of the DMI. Also, the application of a magnetic field generically increases a tendency towards destabilization of the phase. The nature of that phase itself cannot be gauged from our analysis but for our parameter values it is far from the field dominated ordered phases.

Our results in this work are restricted to the leading order calculations of self-energy. The next order effects have in several cases been accounted for using an effective modification to the three boson terms of the interaction Hamiltonian and the associated canting angle renormalization [44,45]. Such higher order effects, though not negligible, are smaller than the leading order effects for fields far away from saturation [45]. In our study, which is on a three-dimensional system with a multiple sublattice structure, we have restricted our analysis to the leading order, considering the higher dimension and the values of the field being far from staturation. On general grounds, considering the subdominant effect at low fields in two dimensions, we expect higher order effects to be weak compared to the leading order effects for those of our parameter regimes where order is stable up to spectral renormalization. Our objective in this work has been to demonstrate the trend of spectral renormalization in a broad range of parameters for a general class of Hamiltonians on the pyrochlore lattice. While the general trends with change in DMI or the fields can be expected to be the same, the precise extent of band renormalization for a given value of DMI and field can differ because of higher order effects.

In this study we have also not addressed the issue of the fate of the topological nature of the band structures with the AIAO phase, which might require nonperturbative techniques close to topological degeneracies as mentioned in the text. However, the significant spectral renormalization we report

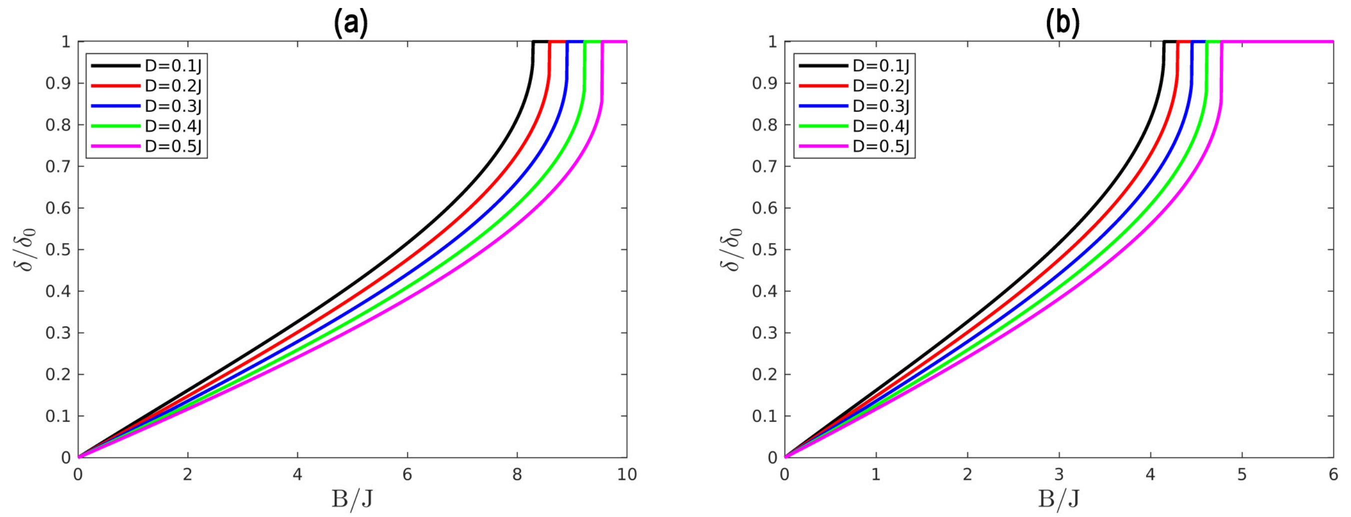

FIG. 8. Variation of the canting (tilt) δ towards the field direction relative to the moment orientation in the AIAO state, when the field is along the [111] direction. δ is effectively the angle between the green and red arrows in Fig. 1 for those spins which are not aligned with the field direction. δ_0 is the angle between the AIAO direction and the field direction. $\delta/\delta_0 = 1$ implies the state fully polarized along the field direction. (a) $S = 1$. (b) $S = 1/2$.

especially along high symmetry directions in the Brillouin zone means that the estimation of the phase boundaries for transitions to such phases might be quite different from those gauged from linear spin wave theory. Finally, our evaluations of the possible parameter regions to probe magnon decay can be extended to give detailed accounts of the channel resolved decay surfaces or the quantitative effect on scattering cross sections. Having established the necessity to take spin wave interactions into account, these more extensive analyses are among the logical next steps for this phase of the pyrochlore lattice.

ACKNOWLEDGMENT

V.R.C. acknowledges funding from the Department of Atomic Energy, India under Project No. RIN 4001-SPS.

DATA AVAILABILITY

Data available from the corresponding author upon reasonable request.

APPENDIX: VARIATION OF CANTING ANGLE WITH THE FIELD

In the main text we discussed the effect of a finite magnetic field on the classical AIAO state which is the lowest energy state in the absence of a field. In Fig. 1(c) we depicted the nature of the classical ground state for a field along the [111] direction. In this case, the three spins of the tetrahedron not aligned with the field tilt towards the field by the same angle δ and the canting happens for each spin in the plane containing the field direction and the initial orientation of the moment. Using these as the defining features of the ground state we can reduce the problem of finding the classical ground state to minimizing the following classical energy function for a given value of $J, D,$ and B.

$$\begin{aligned}
E^{\text{classical}}_{\text{per site}} = {} & \frac{3JS^2}{8} - \frac{3\sqrt{2}DS^2}{8} - \frac{BS}{4} \\
& + \sin(\delta)\left[\sqrt{2}JS^2 - \frac{DS^2}{2} - \frac{BS}{\sqrt{2}}\right] \\
& + \cos(\delta)\left[\frac{BS}{4} - \sqrt{2}DS^2 - \frac{JS^2}{2}\right] \\
& + \sin(2\delta)\left[\frac{DS^2}{4} - \frac{JS^2}{\sqrt{2}}\right] \\
& + \cos(2\delta)\left[-\frac{5\sqrt{2}DS^2}{8} - \frac{7JS^2}{8}\right].
\end{aligned} \tag{A1}$$

The tilt angle corresponding to the classical ground state is the δ corresponding to the minimum of the $E^{\text{classical}}_{\text{per site}}$. It is possible to obtain estimates of the saturation field for this class of states by evaluation of the minima for a range of magnetic fields. The results are shown in Fig. 8 both for $S = 1$ and $S = 1/2$. As expected the canting decreases with the increase in the strength of the DMI and for the figures depicted in the main text the fields are well below the saturation fields. The results of the minimization of the above function do coincide with the numerical minimization results (produced without using any constraints on the spin orientations) used in the main text. We point out here that the above estimates of the saturation fields rely on the specific nature of the magnetic state used, namely coplanarity of the initial and final direction of the moment and the magnetic field direction. We do not know of any proof that the class of minimizing functions will satisfy this property for the entire range of fields depicted in Fig. 8. However, as already mentioned, we rely on unconstrained minimization and for our field values of interest the property holds. An expression like Eq. (A1) can in principle be written for the [100] direction as well using two different canting angles but as it should be clear to the reader it is likely to be considerably more involved and we do not provide explicit expressions for the same.

[1] F. Bloch, Zur Theorie des Ferromagnetismus, Z. Phys. **61**, 206 (1930).

[2] P. W. Anderson, An approximate quantum theory of the antiferromagnetic ground state, Phys. Rev. **86**, 694 (1952).

[3] R. Kubo, The spin-wave theory of antiferromagnetics, Phys. Rev. **87**, 568 (1952).

[4] F. J. Dyson, General theory of spin-wave interactions, Phys. Rev. **102**, 1217 (1956).

[5] F. J. Dyson, Thermodynamic behavior of an ideal ferromagnet, Phys. Rev. **102**, 1230 (1956).

[6] T. Oguchi, Theory of spin-wave interactions in ferro- and antiferromagnetism, Phys. Rev. **117**, 117 (1960).

[7] A. L. Chernyshev and M. E. Zhitomirsky, Spin waves in a triangular lattice antiferromagnet: Decays, spectrum renormalization, and singularities, Phys. Rev. B **79**, 144416 (2009).

[8] M. E. Zhitomirsky and A. L. Chernyshev, *Colloquium*: Spontaneous magnon decays, Rev. Mod. Phys. **85**, 219 (2013).

[9] J. S. Gardner, M. J. P. Gingras, and J. E. Greedan, Magnetic pyrochlore oxides, Rev. Mod. Phys. **82**, 53 (2010).

[10] Y. Onose, T. Ideue, H. Katsura, Y. Shiomi, N. Nagaosa, and Y. Tokura, Observation of the magnon Hall effect, Science **329**, 297 (2010).

[11] P. A. McClarty, Topological magnons: A review, Annu. Rev. Condens. Matter Phys. **13**, 171 (2022).

[12] M. Malki and G. S. Uhrig, Topological magnetic excitations, Europhys. Lett. **132**, 20003 (2020).

[13] H. Kondo, Y. Akagi, and H. Katsura, Non-Hermiticity and topological invariants of magnon Bogoliubov–de Gennes systems, Prog. Theor. Exp. Phys. **2020**, 12A104 (2020).

[14] A. L. Chernyshev and P. A. Maksimov, Damped topological magnons in the kagome-lattice ferromagnets, Phys. Rev. Lett. **117**, 187203 (2016).

[15] S. S. Pershoguba, S. Banerjee, J. C. Lashley, J. Park, H. Ågren, G. Aeppli, and A. V. Balatsky, Dirac magnons in honeycomb ferromagnets, Phys. Rev. X **8**, 011010 (2018).

[16] A. Mook, K. Plekhanov, J. Klinovaja, and D. Loss, Interaction-stabilized topological magnon insulator in ferromagnets, Phys. Rev. X **11**, 021061 (2021).

[17] Y. Liu, L. Zhai, S. Yan, D. Wang, and X. Wan, Magnon-magnon interaction in monolayer $MnBi_2Te_4$, Phys. Rev. B **108**, 174425 (2023).

[18] Q.-H. Chen, F.-J. Huang, and Y.-P. Fu, Damped topological magnons in honeycomb antiferromagnets, Phys. Rev. B **108**, 024409 (2023).

[19] J. Habel, A. Mook, J. Willsher, and J. Knolle, Breakdown of chiral edge modes in topological magnon insulators, Phys. Rev. B **109**, 024441 (2024).

[20] H. Sun, D. Bhowmick, B. Yang, and P. Sengupta, Interacting topological Dirac magnons, Phys. Rev. B **107**, 134426 (2023).

[21] K. Sourounis and A. Manchon, Impact of magnon interactions on transport in honeycomb antiferromagnets, Phys. Rev. B **110**, 054429 (2024).

[22] Y.-M. Li, X.-W. Luo, and K. Chang, Temperature-induced magnonic Chern insulator in collinear antiferromagnets, Phys. Rev. B **107**, 214417 (2023).

[23] J. G. Rau, R. Moessner, and P. A. McClarty, Magnon interactions in the frustrated pyrochlore ferromagnet $Yb_2Ti_2O_7$, Phys. Rev. B **100**, 104423 (2019).

[24] A. Hickey, D. Lozano-Gómez, and M. J. P. Gingras, Order-by-disorder without quantum zero-point fluctuations in the pyrochlore Heisenberg ferromagnet with Dzyaloshinskii-Moriya interactions, Phys. Rev. B **111**, 184434 (2025).

[25] F.-Y. Li and G. Chen, Competing phases and topological excitations of spin-1 pyrochlore antiferromagnets, Phys. Rev. B **98**, 045109 (2018).

[26] P. Laurell and G. A. Fiete, Topological magnon bands and unconventional superconductivity in pyrochlore iridate thin films, Phys. Rev. Lett. **118**, 177201 (2017).

[27] S.-K. Jian and W. Nie, Weyl magnons in pyrochlore antiferromagnets with an all-in-all-out order, Phys. Rev. B **97**, 115162 (2018).

[28] K. Hwang, N. Trivedi, and M. Randeria, Topological magnons with nodal-line and triple-point degeneracies: Implications for thermal Hall effect in pyrochlore iridates, Phys. Rev. Lett. **125**, 047203 (2020).

[29] V. V. Jyothis, B. Patra, and V. R. Chandra, Magnon bands in pyrochlore slabs with Heisenberg exchange and anisotropies, J. Phys.: Condens. Matter **36**, 185801 (2024).

[30] I. Dzyaloshinsky, A thermodynamic theory of "weak" ferromagnetism of antiferromagnetics, J. Phys. Chem. Solids **4**, 241 (1958).

[31] T. Moriya, New mechanism of anisotropic superexchange interaction, Phys. Rev. Lett. **4**, 228 (1960).

[32] T. Moriya, Anisotropic superexchange interaction and weak ferromagnetism, Phys. Rev. **120**, 91 (1960).

[33] R. Moessner and J. T. Chalker, Properties of a classical spin liquid: The Heisenberg pyrochlore antiferromagnet, Phys. Rev. Lett. **80**, 2929 (1998).

[34] R. Moessner and J. T. Chalker, Low-temperature properties of classical geometrically frustrated antiferromagnets, Phys. Rev. B **58**, 12049 (1998).

[35] M. Elhajal, B. Canals, R. Sunyer, and C. Lacroix, Ordering in the pyrochlore antiferromagnet due to Dzyaloshinsky-Moriya interactions, Phys. Rev. B **71**, 094420 (2005).

[36] J. M. Luttinger and L. Tisza, Theory of dipole interaction in crystals, Phys. Rev. **70**, 954 (1946).

[37] T. Holstein and H. Primakoff, Field dependence of the intrinsic domain magnetization of a ferromagnet, Phys. Rev. **58**, 1098 (1940).

[38] J. Colpa, Diagonalization of the quadratic boson Hamiltonian, Physica A **93**, 327 (1978).

[39] A. L. Fetter and J. D. Walecka, *Quantum Theory of Many-Particle Systems* (McGraw-Hill, New York, 1971).

[40] G. C. Wick, The evaluation of the collision matrix, Phys. Rev. **80**, 268 (1950).

[41] A. B. Harris, C. Kallin, and A. J. Berlinsky, Possible Néel orderings of the kagomé antiferromagnet, Phys. Rev. B **45**, 2899 (1992).

[42] O. A. Starykh, A. V. Chubukov, and A. G. Abanov, Flat spin-wave dispersion in a triangular antiferromagnet, Phys. Rev. B **74**, 180403(R) (2006).

[43] P. A. Maksimov and A. L. Chernyshev, Field-induced dynamical properties of the *XXZ* model on a honeycomb lattice, Phys. Rev. B **93**, 014418 (2016).

[44] M. E. Zhitomirsky and T. Nikuni, Magnetization curve of a square-lattice Heisenberg antiferromagnet, Phys. Rev. B **57**, 5013 (1998).

[45] M. E. Zhitomirsky and A. L. Chernyshev, Instability of antiferromagnetic magnons in strong fields, Phys. Rev. Lett. **82**, 4536 (1999).